Czech Technical University in Prague
Faculty of Nuclear Sciences and Physical Engineering

Department of Physics
Experimental Nuclear and Particle Physics

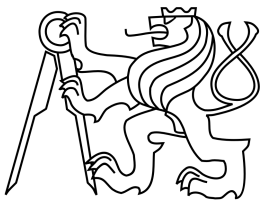

Study of the Dipole Scattering Amplitude using the Balitsky-Kovchegov evolution equation

Author: Marek Matas
Year: 2016

Introduction

Great attention in the previous decade was given to studying the properties of particles at the high-energy limit of QCD. Deep Inelastic Scattering (DIS) studied at the HERA collider was a good tool for measuring such properties. Evolution equations such as BFKL [1–5], BK [6–10], JMWLK [11–15] and DGLAP [16–18] are used to describe the properties of particles that take part in high energy collisions. The BFKL evolution equation predicts the emergence of new partons as the energy of the collision increases. In this approach, at leading logarithmic (LL) accuracy the gluon density is not bound by unitarity restrictions.

In the experiments at large accelerators such as HERA or LHC, it was shown that the number of partons does not completely satisfy this equation and that there are less partons then predicted. Measured cross sections predicted by these evolution equations grow above the experimentally obtained values at high energies, where the largest contribution to the cross section is due to newly created gluons. The fact that predictions from LL-BFKL equation overshoot experimental data may be due to recombination processes inside the hadrons and it is included in the BK evolution equation. Recombination processes take place when it is not anymore energetically favorable for a new parton to emerge in the hadron and its entire phase space is already populated.

The BK evolution equation is an integro-differential equation and there are several ways to solve it numerically [19–22]. The BK evolution equation considered in this work includes running coupling kernel that takes into account the two loop processes and assumes both impact parameter dependent and independent solutions.

Using numerical methods such as the Runge-Kutta method of fourth order and Simpson's rule, one can obtain predictions for the structure functions and reduced cross sections of DIS that include recombination processes within the hadron. Numerical methods used to compute these values need to be studied and an optimal setup regarding the precision and speed of computation has to be tested [23].

The solution of the BK equation depends on the considered initial condition. Currently used initial conditions require several parameters that need to be fitted from data in order to obtain valid predictions for observable quantities. It is desirable to come up with an initial condition that would require less parameters and would correspond to the physical nature of this equation. Geometric scaling [24–27] is a phenomenon that might be used for acquiring such an initial condition . This approach generalizes the evolution of the solution towards higher rapidities and allows us to reverse this evolution back to the starting rapidities and corresponding Bjorken-

x. The properties of this acquired initial condition require only a single parameter that needs to be fitted from data and is obtained solely from the properties of the integro-differential equation itself. However in this approach, the measured structure functions cannot be described in as straightforward way as it was with the original initial condition. The change of the evolution behavior when this initial condition is introduced needs to be studied in order to answer the question of validity of this approach and to determine the new set of computation parameters such as σ_0.

Results obtained by solving this equation can be used in describing and understanding processes that occur in heavy-ion physics, especially on experiments such as LHC or RHIC.

In this work, we first manage to reproduce the results obtained by other theoretical groups both for the impact parameter independent equation [21]. Since these numerical computations are typically CPU-time demanding, we then focused on the optimization of the numerical method. We managed to reduce the running time by more then one order of magnitude after implementing the optimized computation [23]. Then we established an analysis to find and test a new initial condition that would be given by the intrinsic properties of the rcBK equation. The properties of this scaled initial condition proved to be of a different nature then those of the originally considered MV initial condition. We tested those properties and then established the optimal way of obtaining such initial condition. The scaled initial condition was then used to predict values of the structure function in regions where it differs from the MV initial condition.

My personal contribution to the results presented in this thesis is the following:

1. Implementation of the Runge-Kutta method of order one, two and four to solve the rcBK evolution equation.
   (a) The method of order two has already been used in [21], and I have used those results to cross check my implementation.
   (b) The method of order four has been introduced in [22], and I have used those results to cross check my implementation
2. I have searched for the best parameters of the numerical setup to balance the speed of execution with the accuracy of the numerical results. These results are new; they are presented in Section 3.1 and have been reported in [23].
3. I have explored the use of initial conditions obtained from solutions of the rcBK equations at large rapidities using geometric scaling. These results are new. They are discussed in Section 3.3 and are intended for publication in the near future.

This contribution is a subsection to my Diploma thesis that was submitted in the May of 2016.

Chapter 1

High energy collision phenomenology

1.1 Color dipole approach to DIS

So far we have shown how the inner composition of proton changes with respect to energy and scale of the incoming photon.

If we consider the target rest frame, the lepton - hadron collision is as follows. First, the incoming lepton emits a virtual photon. This photon then spontaneously fluctuates into a quark - antiquark color dipole (analog to the dipole in electrodynamics). This dipole then interacts strongly with the target proton and its further fluctuation back into a photon is disrupted. This approach is called the Color dipole model [35–40]. The fluctuation of a photon into the color dipole is necessary because of new particles that emerge from the collision, which is only possible when strong interaction is present and could not be described by mere electromagnetic interaction.

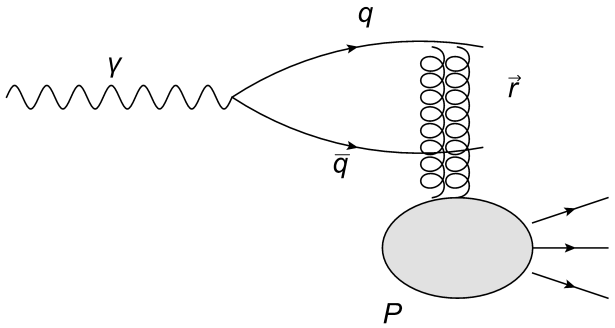

Figure 1.1: Color dipole fluctuating from the virtual photon [41].

At small x, it can be shown that the lifetime of such quark - antiquark fluctuation is greater than the average time of the whole interaction [31], which is important because then the dipole has enough time to react with the target hadron before it annihilates. The cross section of the total photon-proton scattering is shown in 1.1,

where $\mid \Psi^i_{T,L} \mid^2$ is the wave function of the photon that fluctuates to create a color dipole. Indexes T and L correspond to transverse and longitudinal polarizations of the incident photon and e_{q_i}, m_{q_i} and z correspond to fractional electric charge of quark q_i, its mass and fraction of the longitudinal momentum of photon it carries.

$$\sigma^{\gamma^* - h}_{T,L}(x, Q^2) = \sum_i \int d\vec{r} dz \mid \Psi^i_{T,L}(z, \vec{r}) \mid^2 \sigma^{q\bar{q}}(\vec{r}, x) \tag{1.1}$$

The final cross section is then computed by integrating the photon-color dipole wavefunction and the cross section of the quark-antiquark dipole scattering of the proton target over all transverse dipole sizes $\vec{r}$ and over all possible values of photon's fractional momentum z [21].

Using the dipole cross-section $\sigma^{q\bar{q}}(r, x)$ we can compute the structure function F_2 as shown in Eq. 1.2 and this can then be measured experimentally.

$$F_2(x, Q^2) = \frac{Q^2}{4\pi^2 \alpha_{em}} \int \sum_i d\vec{r} dz \mid \Psi^i_{T,L}(z, \vec{r}) \mid^2 \sigma^{q\bar{q}}(\vec{r}, \tilde{x}), \tag{1.2}$$

[22] where $\mid \Psi^i_{T,L}(z, \vec{r}) \mid^2$ is a sum of squared longitudinal and transversal photon wave functions as shown in Eq. 1.4 and $\tilde{x}$ is introduced due to photoproduction limit as shown in Eq. 1.3 [42].

$$\tilde{x} = x \left(1 + \frac{4m^2_{q_i}}{Q^2}\right), \tag{1.3}$$

where the mass of the incident quark is set to the value of $140\,\mathrm{MeV}^2$ for u,d and s quarks. For charm quark, the mass is set to $1.27\,\mathrm{GeV}^2$ and $4.2\,\mathrm{GeV}^2$ for the beauty quark [43].

$$\mid \Psi^i_{T,L}(z, \vec{r}) \mid^2 = \mid \Psi^i_T(z, \vec{r}) \mid^2 + \mid \Psi^i_L(z, \vec{r}) \mid^2 \tag{1.4}$$

and the longitudinal and transversal photon wave functions are given by

$$\mid \Psi^i_T(z, \vec{r}, Q^2) \mid^2 = \frac{3\alpha_{em}}{2\pi^2} e^2_{q_i} ((z^2 + (1-z)^2)\epsilon^2 K^2_1(\epsilon r) + m^2_{q_i} K^2_0(\epsilon r)) \tag{1.5}$$

$$\mid \Psi^i_L(z, \vec{r}, Q^2) \mid^2 = \frac{3\alpha_{em}}{2\pi^2} e^2_{q_i} (4Q^2 z^2 (1-z)^2 K^2_0(\epsilon r)) \tag{1.6}$$

where z is the fraction of the total momentum carried by the quark, K_0 and K_1 are the MacDonald functions and

$$\epsilon^2 = z(1-z)Q^2 + m^2_{q_i}, \tag{1.7}$$

where m_{q_i} is the mass of the considered quark.

The reduced cross-section is obtained from relation [21]

$$\sigma_r(x, y, Q^2) = F_2(x, Q^2) - \frac{y^2}{1 + (1 - y)^2} F_L(x, Q^2), \tag{1.8}$$

where inelasticity y is obtained from $y = Q^2/sx$ and $\sqrt{s}$ is the CMS collision energy.

The actual dipole scattering cross section is then computed by integrating the dipole-proton scattering amplitude over the impact parameter as shown in Eq. 1.9.

$$\sigma^{q\bar{q}}(r, x) = 2 \int d\vec{b} N(x, r, \vec{b}) \tag{1.9}$$

This dipole cross section then covers all the QCD effects and can be also obtained from the BK evolution equation. If we neglect the dependence of the scattering amplitude N on the impact parameter, the integral over it can be simplified into expression 1.10. [44],

$$\sigma^{q\bar{q}}(r, x) = \sigma_0 N(x, r) \tag{1.10}$$

where σ_0 is a parameter that we fit from data.

1.2 Evolution equations

During the interaction, color dipole exchanges a particle with the target hadron. To maintain the color conservation, the exchanged particle must be colorless and in the first approximation we consider it to be a pair of gluons. The actual complex particle that is exchanged is called Pomeron. A linear approach to the interaction such as the one used in BFKL evolution equation suggests only one particle exchange between the color dipole and target hadron whereas non-linear evolution equations such as the BK equations suggest multiple pomeron exchanges.

If we fix the scale of the virtual photon and increase the energy of the collision, we observe that some gluons start to overlap due to fixed dimensions of the proton itself. In this case we have to take into account the recombination processes that take place among gluons as they become more influential. The scale when gluons start to overlap is called saturation scale and occurs when most of the phase space in the proton is already occupied by other gluons. Further decreasing of Bjorken x will then not result into further gluon number rise since the whole system is already saturated and the new gluons are compensated with the recombination processes and a dynamical balance is established. This situation varies for different scales as with higher Q^2, we decrease the dimensions of the gluons themselves. We can determine a so called saturation scale Q_s at which this effect takes place with respect to the total energy. These non-linear recombination processes are described by the Balitsky-Kovchegov evolution equation (BK).

1.2.1 Balitsky-Kovchegov evolution equation

Balitsky-Kovchegov evolution equation (BK) is one of the equations that describe the evolution of the scattering amplitude N. It was derived from the JIMWLK evolution equations in the limit of large number of colors N_c by Kovchegov [10, 49, 50]. It is a modification of the BKFL evolution equation and unlike BFKL, does account for the nonlinear effects of gluon recombination. The BK evolution equation is shown in Eq. 1.11 [51, 52]

$$\frac{\partial N(r,Y)}{\partial Y} = \int d\vec{r_1} K^{run}(r,r_1,r_2)(N(r_1,Y)+N(r_2,Y)-N(r,Y)-N(r_1,Y)N(r_2,Y)), \tag{1.11}$$

where $K^{run}(r,r_1,r_2)$ can be expressed as in Eq. 1.12 [53]

$$K^{run}(r,r_1,r_2) = \frac{N_c \alpha_s(r^2)}{2\pi^2}\left(\frac{r^2}{r_1^2 r_2^2} + \frac{1}{r_1^2}\left(\frac{\alpha_s(r_1^2)}{\alpha_s(r_2^2)} - 1\right) + \frac{1}{r_2^2}\left(\frac{\alpha_s(r_2^2)}{\alpha_s(r_1^2)} - 1\right)\right) \tag{1.12}$$

and $\vec{r_2} = \vec{r} - \vec{r_1}$. If we disregard the last term in the BK equation, we obtain a linear equation that can be shown to be equivalent to the BFKL evolution equation [45]. As the rapidity increases, this linearized version rises the scattering amplitude above any boundaries.

The coupling that is used in the kernel of the integro-differential equation depends on the number of considered quark flavors according to equation 1.13.

$$\alpha_{s,n_f}(r^2) = \frac{4\pi}{\beta_{0,n_f} ln\left(\frac{4C^2}{r^2\Lambda_{n_f}^2}\right)}, \tag{1.13}$$

where

$$\beta_{0,n_f} = 11 - \frac{2}{3}n_f. \tag{1.14}$$

The constant C^2 is the uncertainty coming from the Fourier transformation that was used to derive this result and is usually fit to data [44]. The constant n_f corresponds to the number of flavors that are active, and is usually set to a value of 3 in the light flavor quarks approximation.

$\Lambda_{n_f}^2$ is called the QCD scale parameter and its value depends on the value of n_f in the variable n_f scheme. When heavier quark flavors are active (charm and beauty quark) 1.2.1, its value needs to be calculated from the relation [21]

$$\Lambda_{n_f-1} = (m_f)^{1-\frac{\beta_{0,n_f}}{\beta_{0,n_f-1}}} (\Lambda_{n_f})^{\frac{\beta_{0,n_f}}{\beta_{0,n_f-1}}}. \tag{1.15}$$

fit	Q_0^2	C	$\Lambda^2_{n_f}$	γ	σ_0
GBW	0.241	2.46	0.241	0.971	32.357
MV	0.165	$\sqrt{6.5}$	0.241	1.13	32.895

Table 1.1: A possible values of the initial condition parameters [21].

To determine the value of Λ_5, the experimentally measured value of $\alpha_s(M_Z) = 0.1196 \pm 0.0017$ at the Z^0 mass $M_Z = 91.18\,\text{GeV}$ [54] and the Eq.1.13 can be used. Value of n_f are set for values of r^2 for which the momentum scale is heavier then the heaviest quark considered. This condition can be expressed as

$$r^2 < \frac{4C^2}{m_f^2}. \tag{1.16}$$

Since all dipole sizes are accounted for in the BK evolution equation, there is a need to reduce the coupling after a certain value is reached, so that the maximal value of coupling constant would not exceed a set limit [21, 44]. The modified running coupling takes into account the next to leading two loop expressions [33].

In order to compute the Balitsky Kovchegov evolution equation and get the cross section of the whole interaction or a structure function of a hadron, one must start with certain initial conditions. One of the frequently used initial conditions is the GBW initial condition Eq. 1.17 [44].

$$N^{GBW}(r, x = x_0) = 1 - exp\left(-\frac{(r^2Q_0^2)^\gamma}{4}\right) \tag{1.17}$$

Another typical initial condition for the BK equation is a MV initial condition 1.18 [55]

$$N^{MV}(r, x = x_0) = 1 - exp\left(-\frac{(r^2Q_0^2)^\gamma}{4} ln\left(\frac{1}{r\Lambda} + e\right)\right) \tag{1.18}$$

Where Λ represents the infrared cutoff of the dipole cross section and does not have to be equal to $\Lambda^2_{n_f}$ introduced earlier [44], Q_0^2 is the scale for the biggest Bjorken x that is considered in the computation and γ is a parameter that controls the slope of the fall of the dipole amplitude when r is decreased. However the BK evolution equation does not incorporate the quantum fluctuations of the gluon field and therefore its saturation scale is not entirely accurate. The fluctuations are not accounted for in the fixed coupling approach. The running coupling approach shown in Eq. 1.13 evens its effects out [45]. Table 1.2.1 shows possible values for the initial parameters.

Chapter 2

Solving the rcBK equation

2.1 Impact parameter independent rcBK equation

The Balitsky-Kovchegov equation unfortunately does not have an analytic solution, so it has to be solved numerically such as in [19–21]. A usual way of solving this equation involves the Simpson method for integration, a linear interpolation for acquiring values of $N(r)$ for intermediate positions and the Runge-Kutta method for solving the differential equation.

Since both the Simpson method and the Runge-Kutta method use points in grid and not continuous functions, the initial condition is computed on an equidistant grid with step h. We choose to set a logarithmic grid over the dipole distance vector $\vec{r}$ (and later also for the impact parameter $\vec{b}$) To obtain the next step in rapidity evolution, one must use the RK method and therefore compute the integral

$$\int d\vec{r_1} K^{run}(r, r_1, r_2)(N(r_1, x) + N(r_2, x) - N(r, x) - N(r_1, x)N(r_2, x)). \tag{2.1}$$

This integral depends on the value of r, so it is necessary to compute it for every value of r on the whole considered interval separately. To compute this integral, Simpson method was used. That means that for every value of r, a cycle has been run for the whole interval integrating the function over $\vec{r_1}$, where the value of r_2 was computed according to

$$r_2 = \sqrt{r^2 + r_1^2 - 2rr_1 cos(\theta_{rr_1})} \tag{2.2}$$

where θ_{rr_1} is the angle between $\vec{r}$ and $\vec{r_1}$. If the point r_2 does not match exactly one of the grid points on which the values of the initial condition has been computed, it is necessary to interpolate. Lagrange interpolation of first or third order is considered since even values of interpolations order tend to inaccurately interpolate linear regions.

For every point r_1 inside the integral 2.1, integral over θ_{rr_1} has been computed. This variable goes from 0 to 2π but since cosine is an even function, we can simplify this by integrating over $[0, \pi]$ instead and multiplying the result by a factor of two. Once the function is integrated over θ_{rr_1} in every point r_1, it is possible to integrate these integrated functions and determine the final integral. This integral can be split in three separate terms:

$$\begin{aligned} Kernel &= \int d^2\vec{r_1} K^{run}(r_1, r_2, r) \\ Split &= \int d^2\vec{r_1} K^{run}(r_1, r_2, r)(N(Y, r_1) + N(Y, r_2)) \\ Recomb &= \int d^2\vec{r_1} K^{run}(r_1, r_2, r)(N(Y, r_1)N(Y, r_2)), \end{aligned} \tag{2.3}$$

which allows us to speed up the Runge-Kutta method. These three terms are then used to compute the next step in the rapidity evolution and this step is then added to the initial condition in every point of r. The obtained function be used as an input to this process until the desired rapidity is reached.

To speed up this process, it is useful to create a three-dimensional array in the very beginning of the computation that will hold the values of $K^{run}(r, r_1, r_2)$ for every combination of r, r_1 and r_2 so that they don't have to be computed over and over. Same principle was used to hold the values of $r_2(r, r_1, \theta_{rr_1})$.

To determine the values of $\alpha_{run}(r^2)$, equation 1.13 is used on a region, where $r > r_{run}$ holds. The value of r_{run} is chosen so that the total value of $\alpha_{run}(r^2)$ would never exceed the value of 0.7 [21].

For some choices of r, r_1 and θ_{rr_1} the value of $K^{run}(r, r_1, r_2)$ diverges. It is then necessary to exclude these points from the whole integral, because whereas in continuous integration a diverging singularity does not necessarily mean divergence of the entire integral, in the discrete approximation an infinite value added to the integration sum changes the result irreversibly.

2.2 Geometric Scaling

The solution of the BK evolution equation exhibits a phenomenon called Geometric scaling [24]. After a few units of rapidity, the initial condition is "forgotten" by the evolution and the solution propagates independently. Moreover, as rapidity increases, its geometric properties do not change, the solution only shift towards lower values of r. This then allows us to either predict future values of the evolution, or "rewind" back the evolution and hope to obtain a new initial condition to this integro-differential equation, that would require less parameters and that would be obtained solely from the intrinsic properties of the BK equation. The evolution of the solution to the BK equation is shown in Fig. 2.1 where we can see the effect of geometric scaling.

The evolution equation itself forgets the shape of the initial condition in the evolution

in few units of rapidity. Even if we choose to start with dramatically different initial conditions, by the rapidity $Y = 8$ the solution yields its usual shape.

Figure 2.2 shows the evolution for a simple linear initial condition that has a value of 0 for all dipole sizes below 1, linearly grows to one in the (1,10) interval and has a value of 1 elsewhere. Even more extreme initial condition was considered in Figure 2.3, that shows the evolution for an initial condition that exceeds the value of 1 for $N(r, Y)$. It has a value of 0 for r smaller then 1, linearly grows up to the value of 1.5 at the dipole size of twenty, and is set to 1 for larger dipole sizes. Final initial condition that was tested is shown in Fig. 2.4. It does not reach the value of one for $N(r, Y)$ anywhere on the interval and is set to 0 for the dipole sizes smaller than one, grows linearly to the value of 0.5 at $r = 5$ and stays at that value for the remaining part of the interval. Note that the dipole size axis is in the logarithmic scale.

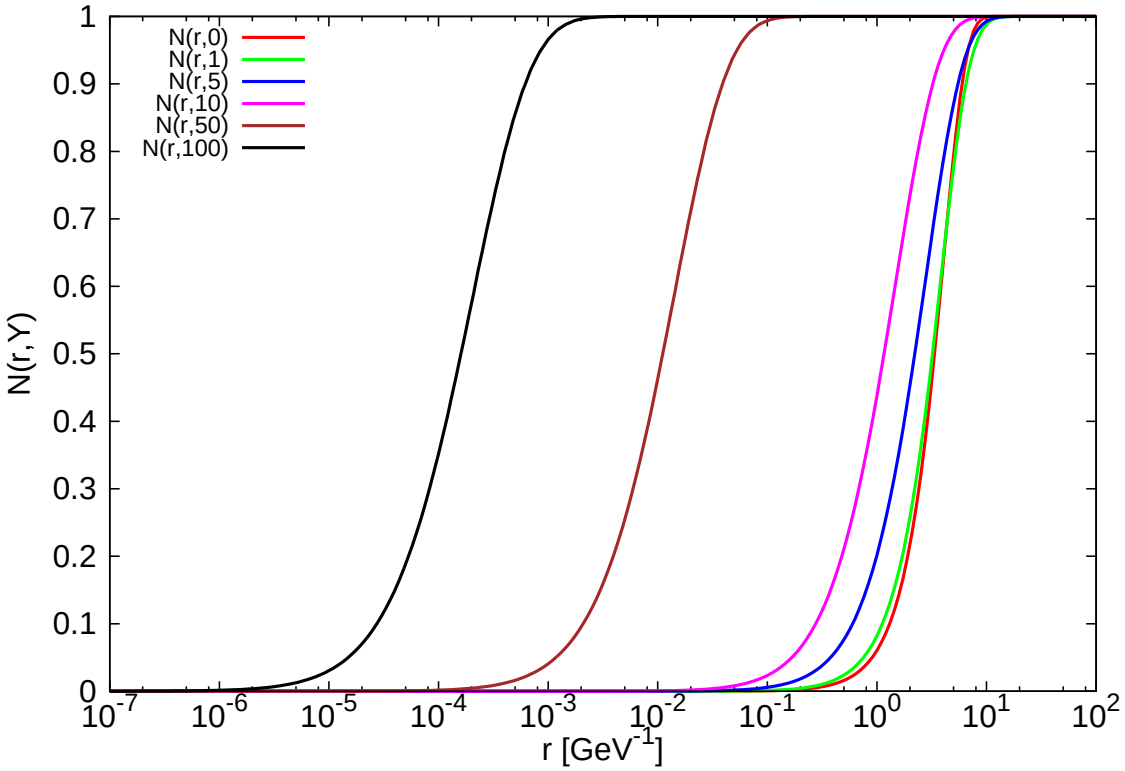

Figure 2.1: The shape of the solution to the BK equation shows geometric scaling properties.

We can see that these extreme initial conditions seem not to affect the later evolution and that the evolution equation itself shapes the curve into a predetermined shape. In all of these cases we can see that by rapidity of about 10, the shape of the initial condition is suppressed and that the evolution than continues similarly for all initial conditions.

For obtaining the geometrically scaled solution, we ran the MV initial condition to high rapidity ($Y = 100$) where the integro-differential equation "forgot" the shape of the initial condition and then re-scaled it to the starting value.

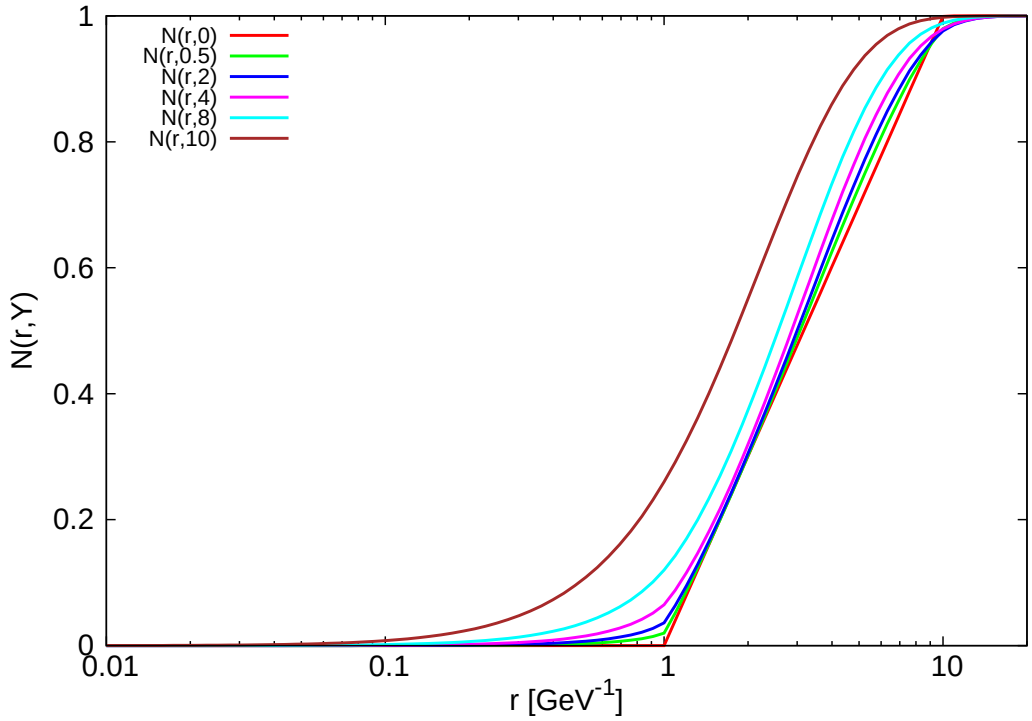

Figure 2.2: Evolution of N(r,Y) when a simple linear initial condition is used.

First, we found r_s^{100} according to the condition.

$$N(r_s^{100}, Y = 100) = 0.5, \tag{2.4}$$

and then we computed the value of r_s^0 from the saturation scale as

$$Q_{s0} = 1/r_s^0. \tag{2.5}$$

The saturation scale Q_{s0}^2 is a free parameter that needs to be fitted from the data. Since for such obtained value of r_s^0 stands

$$N(r_s^0, Y = 0) = 0.5, \tag{2.6}$$

we then calculated the shift in the r-axis in logarithmic scale according to

$$\Delta r = ln(r_s^{100}) - ln(r_s^0) \tag{2.7}$$

and then re-scaled the solution to the rcBK equation as

$$N(ln(r), Y = 0) = N(ln(r) - \Delta r, Y = 100). \tag{2.8}$$

We linearly interpolated when the values of $ln(r) - \Delta r$ got of the precomputed grid.

The initially considered value for the saturation scale was set as $Q_{s0}^2 = 0.07\,\mathrm{GeV}^2$. The values of $\frac{F_2 data}{F_2 rcBK}$ were evaluated and fitted with a constant to determine the new value of σ_0 since the original value obtained with MV initial conditions can differ. A second propagation to $Y = 100$ and re-scaling of the initial condition was carried out to determine the validity of the assumption that by $Y = 100$, the rcBK equation "forgot" its initial condition.

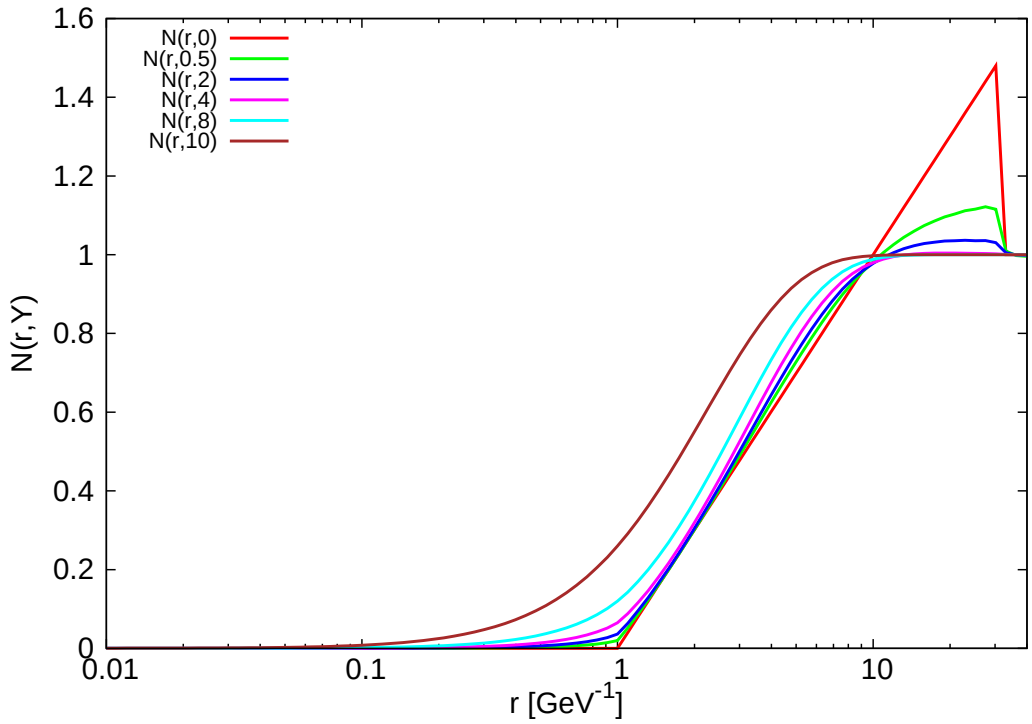

Figure 2.3: Evolution of N(r,Y) when an atypical initial condition is used, that exceeds the value of one.

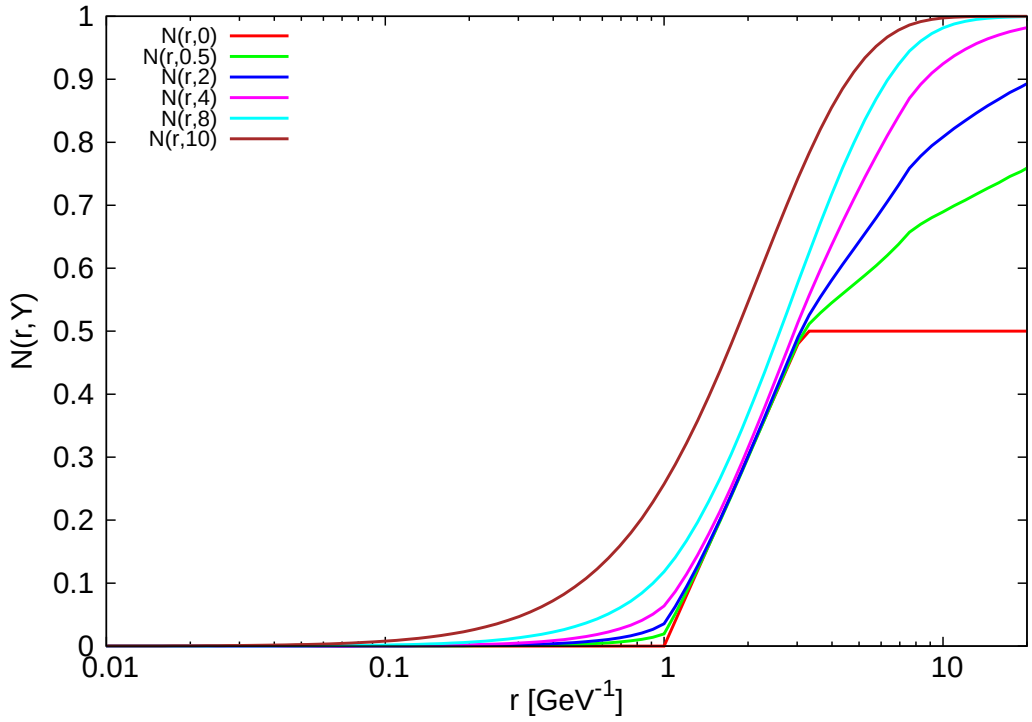

Figure 2.4: Evolution of N(r,Y) when an atypical initial condition is used, that does not reach one.

Chapter 3

Results

3.1 The Optimal Setup

To find the optimal setup of parameters that are used throughout the computation, their influence on the result has been analyzed [23]. For each parameter, it was necessary to find a reasonable ratio between precision and running time of the computation. Therefore each parameter has been varied and the amount of change to the resulting function was studied.

As a default computation setup, the MV initial condition with the value of parameters shown in Tab. 3.1 were used in the Runge-Kutta method of fourth order, 25 steps over each order of magnitude in r, 10 steps in the interval of $[0, \pi]$, 10000 steps in the integration over the interval [0,1] of z in the photon wave function computation, linear interpolation method and a step of 0.01 over Y in the Runge-Kutta method.

The variations of the type of method where the Runge-Kutta method of fourth order, the Ralston method and the Euler method have been compared. We showed that the difference between results obtained by the Euler and RK2 methods is about twice as high as the difference between the RK2 and RK4 methods and is of the order of one percent of the total value. However the difference between the running times for the Euler method and the RK4 method is not as significant and therefore we will restrict ourselves to the RK4 in the following computations.

A variation for the integration step over the parameter θ_{rr_1} has been done. Steps of 5, 10, 20 and 40 have been compared at various rapidities to determine the optimal speed/precision ratio. The variation of the scattering amplitude when five steps over the interval of $[0, \pi]$ are considered instead of 10 reaches up to 25% for the rapidity of $Y = 10$ and decreases slowly with rising dipole size r. The change of the resulting

Fit	Q_0^2	C	$\Lambda_{n_f}^2$	γ	σ_0
MV	0.165	2.52	0.241	1.135	32.895

Table 3.1: Parameters for the default MV initial condition [21].

function when 20 steps are introduced instead of 10 over $[0, \pi]$ starts with a value of about 1% for the rapidity of 10 but decreases rapidly with increasing r. As we will see further in the thesis, the small values of r are not as important for the comparison to the experimental data because of the behavior of the wave function term. Increasing the steps further results in an even smaller variation of the scattering amplitude.

A variation over the integration step r has been done. The values of 10, 25, 50 and 100 per order of magnitude were compared. We have shown that the difference between the result obtained by the method using 10 steps per order of magnitude and 25 steps exceeds the value of 2% on the central part of the interval for the rapidity of 10. This region is particularly important for the precision of the obtained result as shown in the following section. When we use 50 steps per order of magnitude, the difference between the results obtained with 25 is less than 1% for most of the interval with the exception of values of r smaller then 10^{-6}. The scattering amplitude variation when 100 steps per order of magnitude are introduced has also less then 1% difference when compared to the previous 50 steps method.

Various methods of interpolation have been tested. As it turns out, the cubic interpolation is not good for this computation since it does not describe well the regions where the slope changes rapidly and an error is introduced into the evolution. For the evolution with the use of cubic interpolation, we have shown that in some regions, the value of $N(r, y)$ exceeds the value of one, which is violating the fact that its value have to fall within the [0,1] interval.

The step of the Runge-Kutta method has also been varied. The obtained scattering amplitude can differ by 4% at rapidity $Y = 10$ when steps of 0.05 and 0.01 are compared, for further interval splitting (from 0.01 to 0.005) the scattering amplitude variation does not exceed the value of 0.6% at the rapidity of 10.

Therefore we conclude that for our case, we will restrict ourselves to use the set of computation parameters for the impact parameter independent rcBK as follows. Runge-Kutta method of fourth order, linear interpolation, a step in rapidity of 0.01, 25 steps over the order of magnitude in r and 10 steps over the interval $[0, \pi]$ in the integration over θ_{rr_1}. We will assume that the b-dependent rcBK equation would exhibit a similar behavior since the methods and numerical complexity of the computation does not change.

3.2 rcBK solutions without impact parameter dependence

The Balitsky Kovchegov evolution equation was used to obtain the following results combined with Simpson's rule for integration and the Runge-Kutta method of fourth order for solving the differential equation.

The properties of the photon wave function $\mid \psi_{T,L} \mid^2$ weighted with several factors that are needed to compute the proton structure function and reduced cross section are shown in the following figures as well as the evolution of $N(r, Y)$ with respect

to rapidity and r. Fig. 3.2 shows the dependence of $\mid \psi_{T,L} \mid^2$ on r for different values of Q^2.

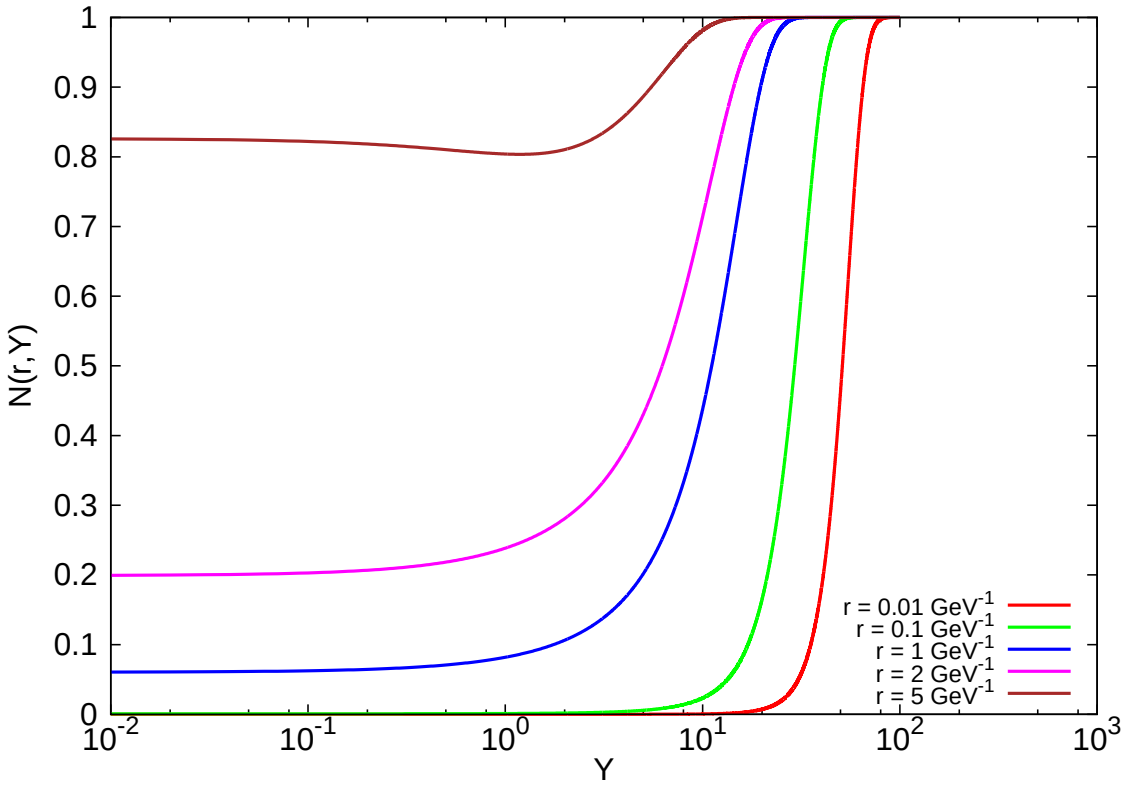

Figure 3.1: The dependence of $N(r, Y)$ on Y for various values of r.

To obtain the structure function $F_2(x, Q^2)$ for the b-independent case, it is only needed to integrate the function shown in Fig. 3.3 and multiply it by a constant factor. This function reaches a value of 10^{-8} at $r = 0.01$ GeV^{-1}, which is below its maximum value by a factor of 10^{-4}. Similar situation occurs at $r = 40$ GeV^{-1}. So the region of the main interest and desired precision for obtaining an accurate value of $F_2(x, Q^2)$ is $r \sim (0.1, 30)$ GeV^{-1}.

Figures 3.4 and 3.5 show the predicted values of the structure function and the reduced cross section for the b-independent case compared with the data from HERA.

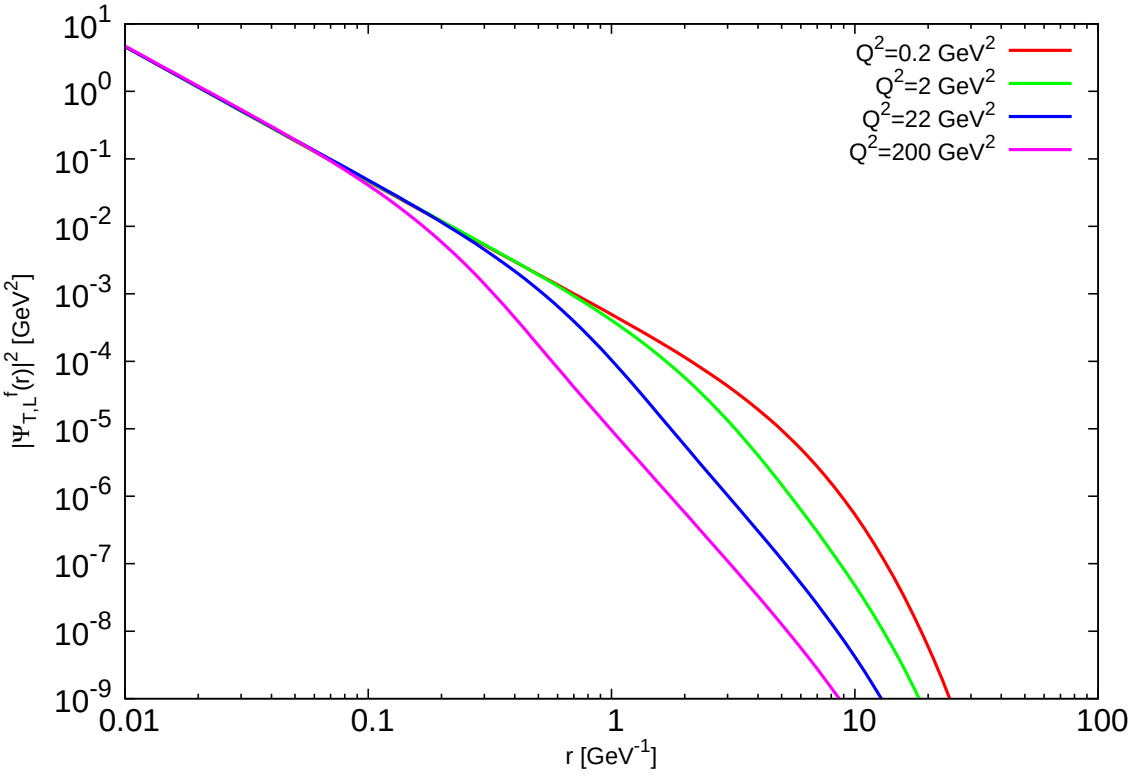

Figure 3.2: The photon wave function $\mid \psi_{T,L} \mid^2$ integrated over z.

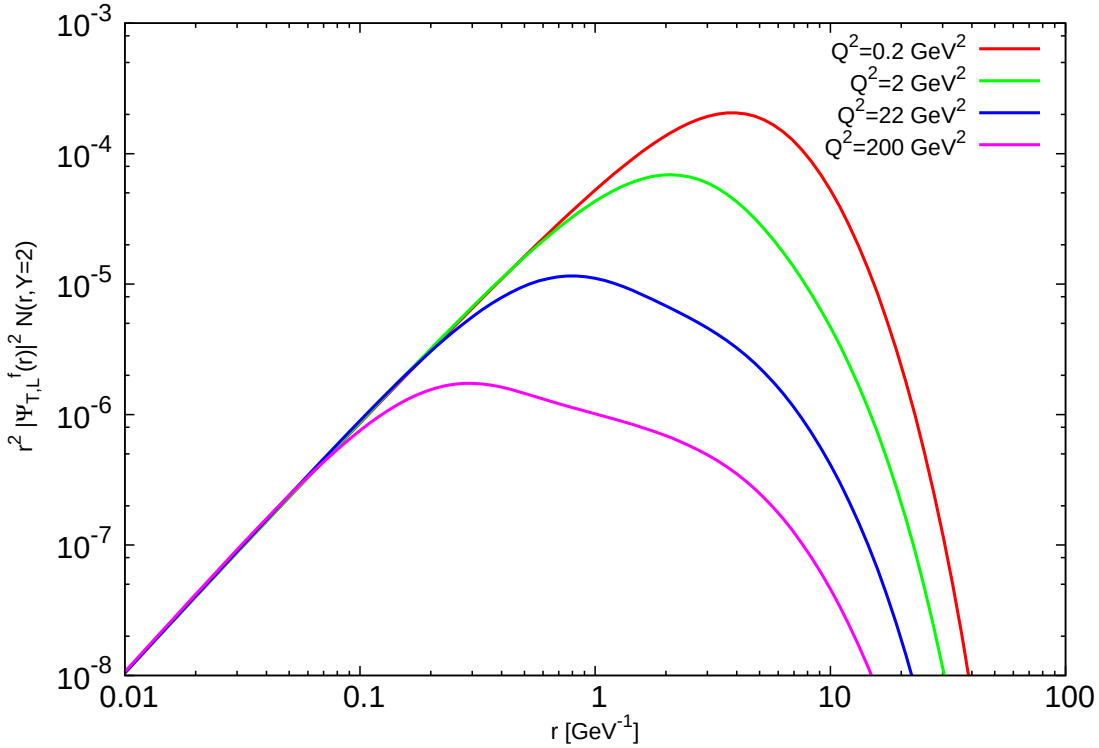

Figure 3.3: The photon wave function $\mid \psi_{T,L} \mid^2$ multiplied by the scattering amplitude $N(r, Y)$ and r^2 for various values of Q^2.

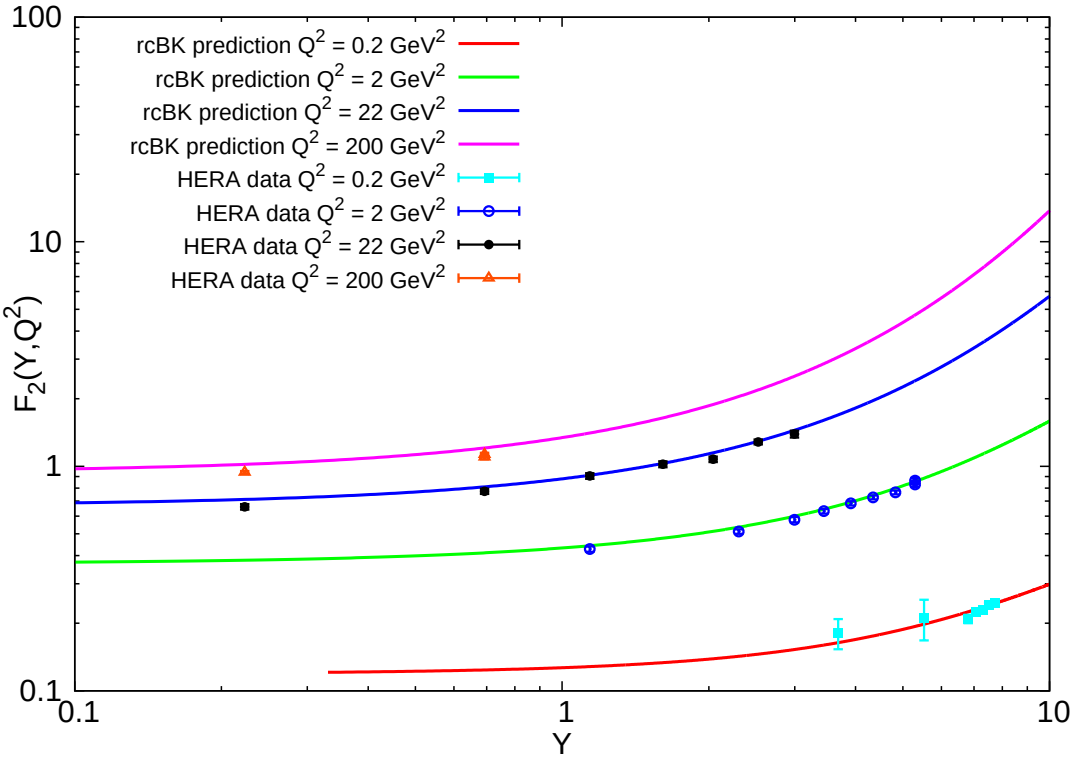

Figure 3.4: The dependence of the proton structure function $F_2(Y, Q^2)$ on Y and compared with data from HERA [56].

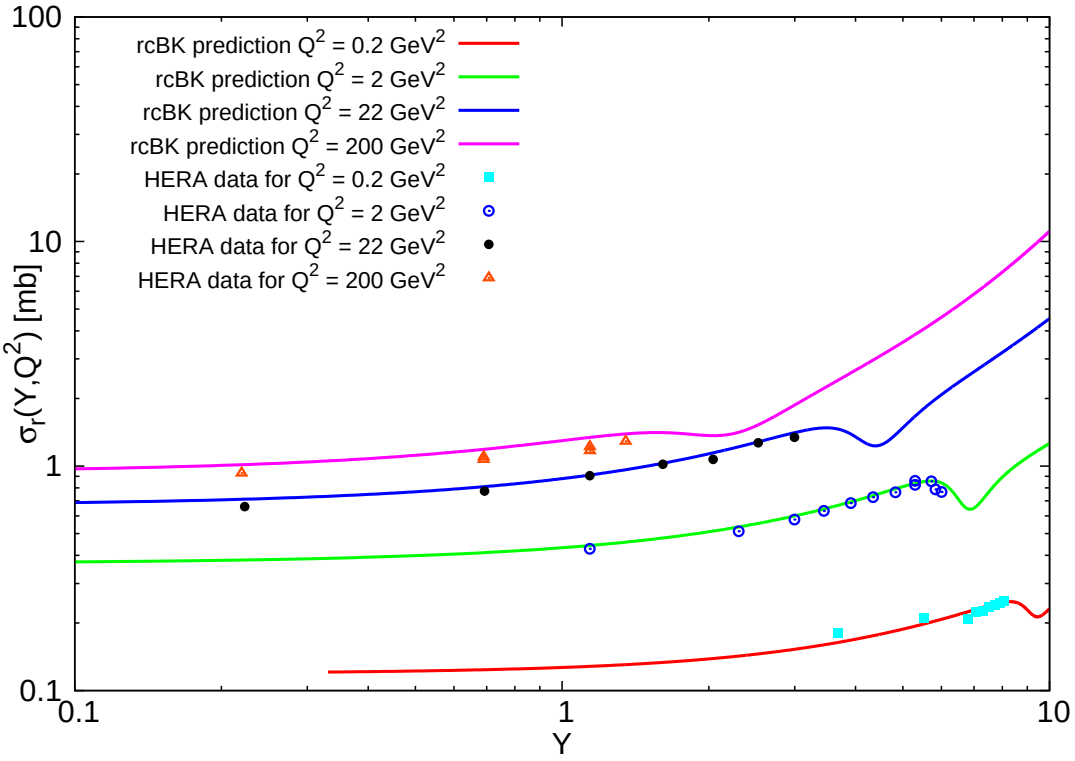

Figure 3.5: The dependence of the reduced cross section $\sigma_r(Y, Q^2)$ on Y compared with data [56].

3.3 Geometric scaled solutions

In this section, I will discuss the process of finding a geometrically scaled initial condition. First, we took the MV initial condition with parameters described in previous sections and ran the evolution to $Y = 100$. For larger values of rapidity, the solution does not change its shape with further evolution, but just shifts along the r-axis. By the rapidity of $Y = 100$, we assumed that the evolution already forgot the MV initial condition since as was shown in the previous section, even dramatically different initial conditions converge to the usual shape by the rapidity of 8. This scaled solution was then taken and re-scaled to higher values of r to obtain a new initial condition that would be more physical and require less parameters that need to be fitted from data.

In the re-scaling process, we had to come up with a parameter, that would characterize the amount of shift in the values of r. This parameter is called Q_{s0}^2 and it determines the amount of shift according to the equation by the relations

$$Q_{s0} = 1/r_0 \tag{3.1}$$

and

$$N(r_0) = 0.5. \tag{3.2}$$

The initially considered value was $Q_{s0}^2 = 0.07\,\mathrm{GeV}^2$ which was later varied. For this re-scaled initial condition, we ran the evolution again to $Y = 10$ to get the observable values that can be compared to the data measured at HERA.

Figure 3.6 compares the geometrical scaled initial condition to the MV initial condition. We can see that the geometric scaled initial condition is different to the MV initial condition that was obtained by fitting the data in the range that is of the most importance.

Since we now used a different initial condition, the previously used value of σ_0 which parametrizes the integral over b in the approximation of a trivial black disc b-dependence might have a completely different value and needs to be fitted from data again. To obtain this fit, we computed the values of F_2^{Data}/F_2^{Theory} for values of Q^2 varying from 0.2 to 150 GeV^2. For each value of Q^2, we fitted the ratio of structure functions with a constant to determine the correction factor for the previously used value of σ_0.

This ratio then showed a nontrivial Q^2 dependence. Its value obtained from the constant fit was decreasing in a logarithmic-like decrease see Fig. 3.7. We then varied the initial re-scaling parameter Q_{s0}^2 from the values of 0.03 to $0.13\,\mathrm{GeV}^2$ to determine the dependence of this logarithmic decrase on the shift of the intial condition. The results for the values of $Q_{s0}^2 = 0.04$ and $0.13\,\mathrm{GeV}^2$ are shown in Fig. 3.7 and 3.8 respectively. As we can see, the slope of the logarithmic decrease remains the same, only a constant shift towards the lower values of the ratio is observed, when we go to higher values of Q_{s0}^2.

Of course in this approach, we assumed that there is no dependence of the ratio F_2^{Data}/F_2^{Theory} on rapidity. In other words, that the geometrical scaled initial condi-

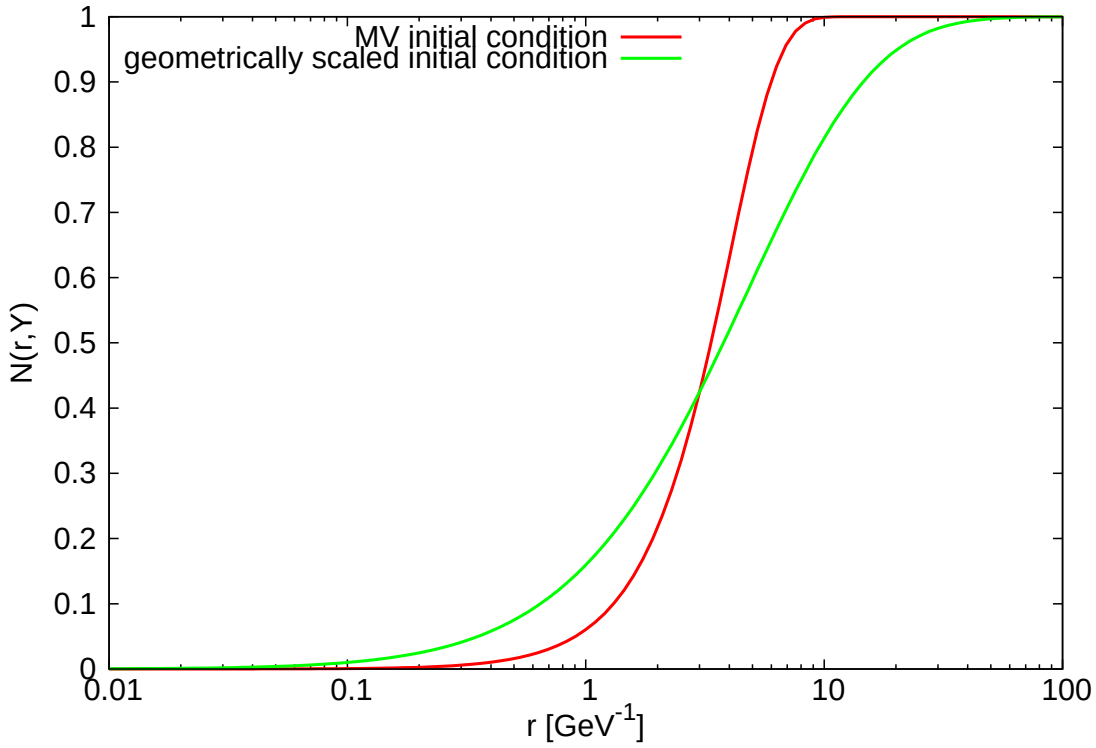

Figure 3.6: MV initial condition and geometrically scaled initial condition with $Q_{s0}^2 = 0.07\,\mathrm{GeV}^2$.

tion predicts the measured values of the structure function correctly and that there are no other effects to be accounted for except for the normalization of the integral over the impact parameter. Therefore next, we focused on determining quantitatively the quality of the fits of F_2^{Data}/F_2^{Theory}. To determine this "validity" of the fit, we used the value of χ^2 which is defined by the following expression

$$\chi^2 = \frac{1}{ndf}\sum_i \frac{(X_i - f(X_i))^2}{\sigma_i^2}, \tag{3.3}$$

where X_i are the measured values and $f(X_i)$ is the value of our fit for the data point X_i. Here σ_i represents the error corresponding to the measured value X_i and ndf stands for the number of degrees of freedom of the fit. The value of χ^2 should be about one for a good fit. If the value is too big, it means that the experimental values are off the describing function and the fit might be incorrect. If the values of χ^2 are too small, it can mean that the errors of the measurement are in fact much smaller than the values used in the computation. The error that we used for our computation was

$$\sigma_i = Er_i\% \frac{F_{2i}^{Data}}{F_2^{Theory}} \cdot 0.01, \tag{3.4}$$

where $Er_i\%$ is the error of the HERA data point i in percent. The values of χ^2 for the values of $Q_{s0}^2 = 0.04$ and $0.13\,\mathrm{GeV}^2$ are shown in Fig. 3.9 and 3.10 respectively.

The fits F_2^{Data}/F_2^{Theory} exhibit rather large values of χ^2 for all possible setups of Q_{s0}^2. If we go towards lower values of Q_{s0}^2 (at about $0.04\,\mathrm{GeV}^2$), the fits get better

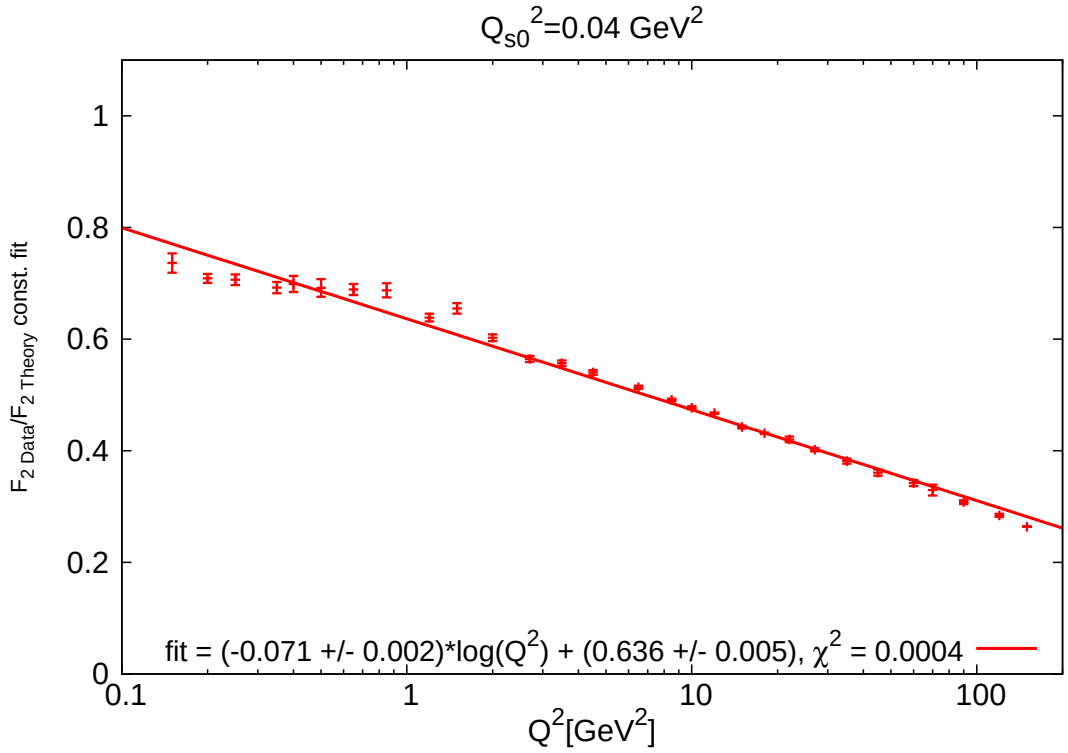

Figure 3.7: The values of fitted F_2^{Data}/F_2^{Theory} with a constant for all Q^2 for $Q_{s0}^2 = 0.04\,\mathrm{GeV}^2$.

in the region of high Q^2 - above $Q^2 = 30\,\mathrm{GeV}^2$, but reach higher values of χ^2 for fits with lower values of Q^2. On the other hand, if we set Q_{s0}^2 to higher values (at about $0.13\,\mathrm{GeV}^2$), the fits get worse in the region of high Q^2, but better in its lower values see Fig.3.9 and 3.10. The studied χ^2 values for the re-scaling parameter spanning from $Q_{s0}^2 = 0.03\,\mathrm{GeV}^2$ to $0.13\,\mathrm{GeV}^2$ lead us to the conclusion that the optimal value lies around the value of $0.07\,\mathrm{GeV}^2$, where the lower values of Q^2 still exhibit reasonable values of χ^2 and the peak forming at higher values does not grow too much to start influencing the values of Q^2 in its proximity.

Even the fits in this region are not perfect constants and the values of F_2^{Data}/F_2^{Theory} show a slight dependence on rapidity. The dependence of the ratios proves to be slightly linearly growing with increasing rapidity, and it may tell us that there are some effects that were not yet accounted for in this approach. This slight growing tendency of the ratios with higher rapidity values is distorting the fits and therefore increasing the resulting value of χ^2. The fact that a small variation from the constant behavior can produce high values of χ^2 is given by the decreasing trend of the errorbar value of the measured data from HERA at higher values of Q^2. As was shown, this behavior cannot be easily singled out by another choice of the re-scaling parameter Q_{s0}^2.

Of course since the evolution is carried out to such high values of rapidity, more error would come from the numerical implementation of the equation (rounding errors, repeated linear interpolation and extrapolation etc.). In order to determine whether the evolution itself can introduce errors that would change the behavior of the scaled

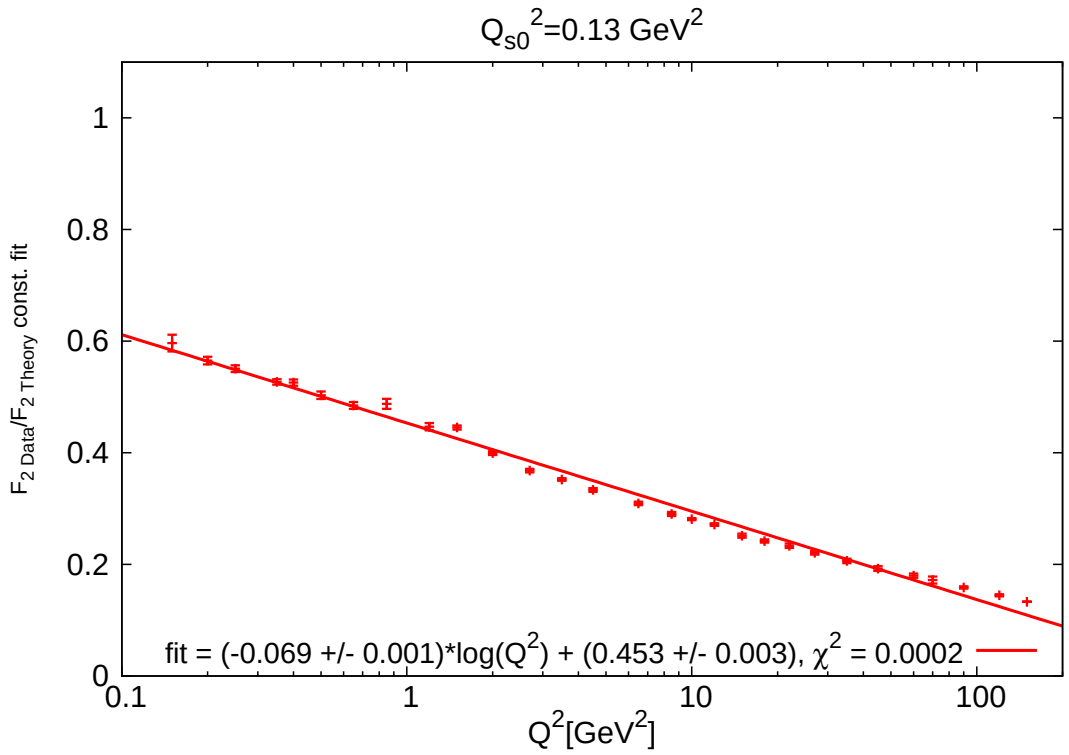

Figure 3.8: The values of fitted F_2^{Data}/F_2^{Theory} with a constant for all Q^2 for $Q_{s0}^2 = 0.13\,\mathrm{GeV}^2$.

initial condition, we took the already scaled initial condition and ran it to $Y = 100$ again. Then we re-scaled it back to the initial position and analyzed its properties in the same manner as was described above for the once-scaled initial condition. The initial condition scaled after running to $Y = 200$ exhibits the same behavior as the initial condition scaled at $Y = 100$. It gives the same logarithmic decrease in the structure function ratio with respect to Q^2 and the χ^2 plots for various values of Q_{s0}^2 are almost identical. The only difference is a slight constant shift of about 0.06 towards lower values of the fit of the structure function ratio which is due to rounding errors and inaccurate interpolations within the computation. It gives us an information on the inaccuracies that are introduced to the solution by computing it up to the rapidity of $Y = 100$.

In order to determine whether this scaled initial condition is of a more physical nature than the initial condition obtained by fitting the data, a prediction of the observables has been made. In Figures 3.11 and 3.12, we can see structure functions computed with both the scaled initial condition and the MV initial condition. The correction factor for σ_0 has been incorporated into the structure function computation for the geometrical scaled case. In these figures we can see the structure function for $Q^2 = 0.25$ and $22\,\mathrm{GeV}^2$ and we can see that they differ in the regions where data has not yet been measured. A future measurement, possibly at the LHC, can determine the validity of this approach to the dipole model and the rcBK evolution equation in particular.

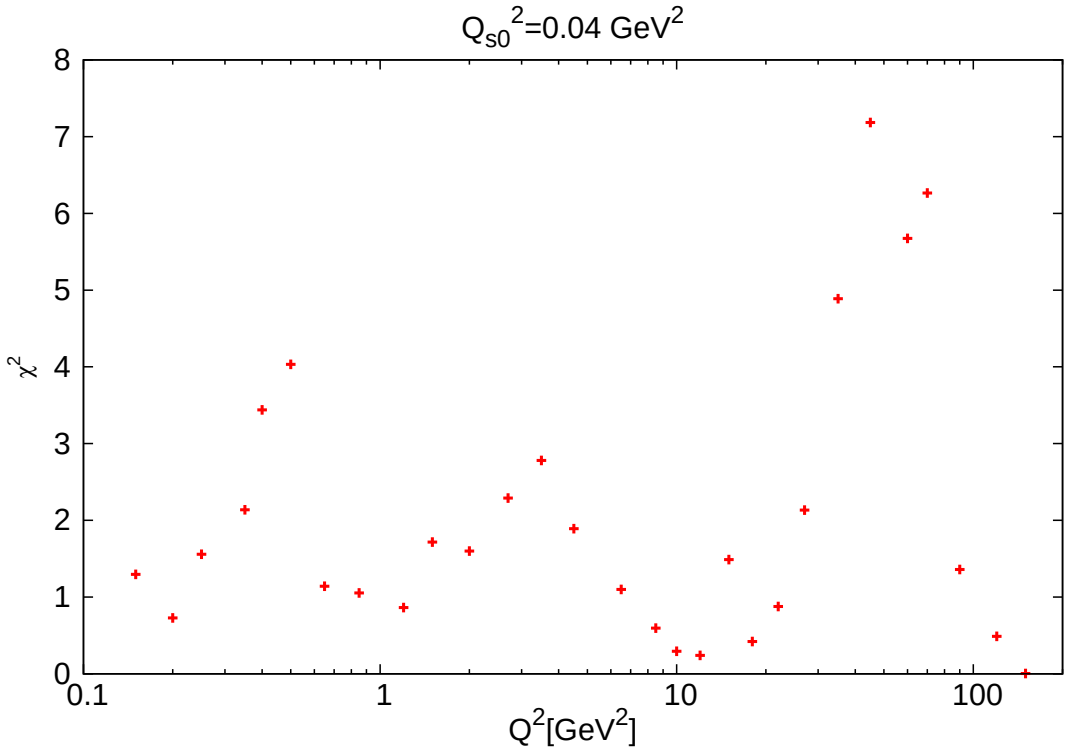

Figure 3.9: The values of χ^2 for all Q^2 for $Q_{s0}^2 = 0.04\,\mathrm{GeV}^2$.

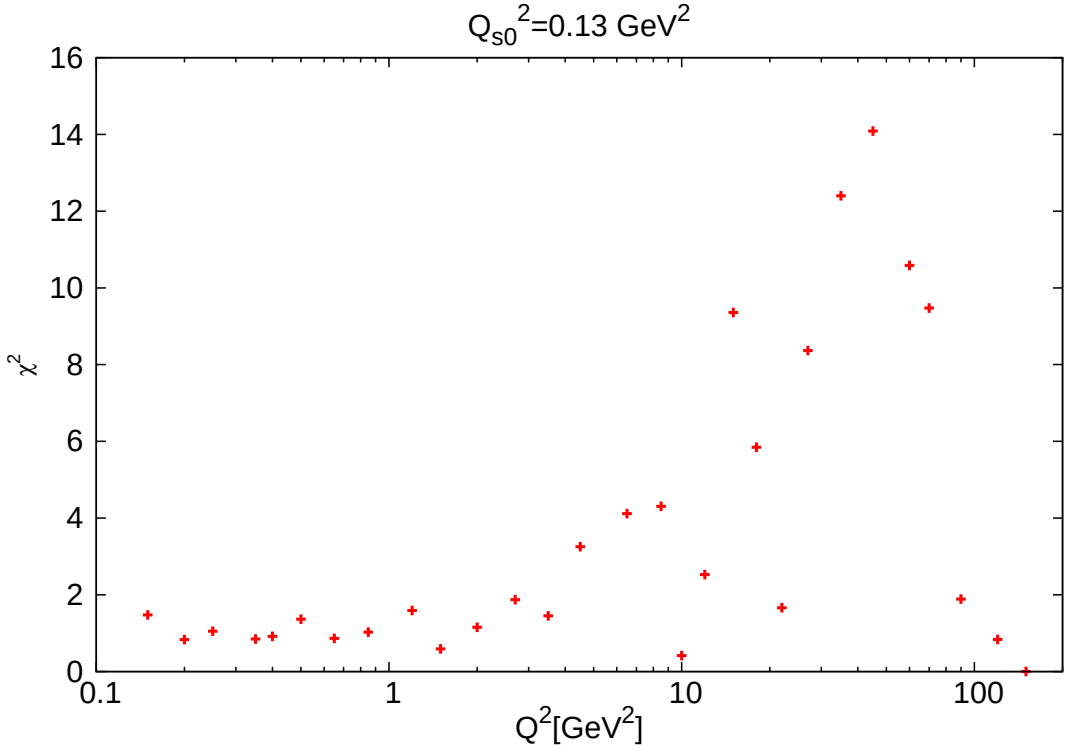

Figure 3.10: The values of χ^2 for all Q^2 for $Q_{s0}^2 = 0.13\,\mathrm{GeV}^2$.

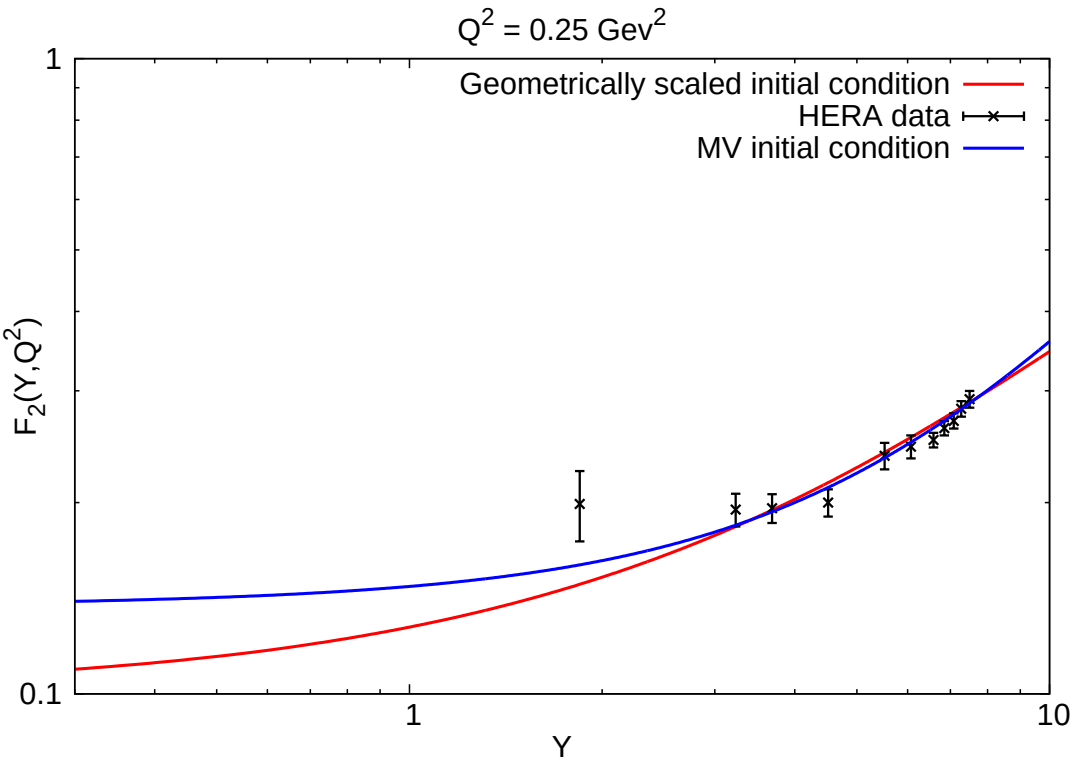

Figure 3.11: The values F_2 for both the MV initial condition [21] and the geometric scaled initial condition obtained with $Q_{s0}^2 = 0.07\,\mathrm{GeV}^2$. Q^2=0.25 GeV^2.

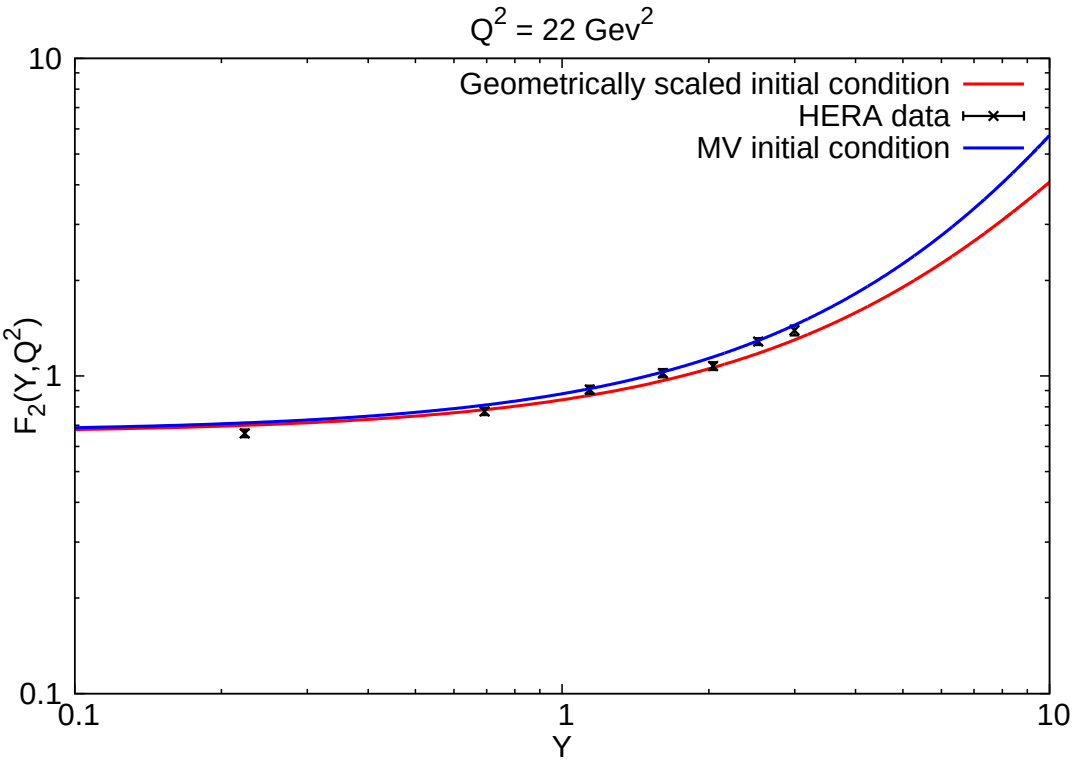

Figure 3.12: The values F_2 for both the MV initial condition [21] and the geometric scaled initial condition obtained with $Q_{s0}^2 = 0.07\,\mathrm{GeV}^2$. Q^2=22 GeV^2.

Conclusion

There are several models that predict the effect of saturation of partons in high energy collisions. The Balitsky Kovchegov evolution equation does that by modifying the BFKL equation with recombination processes that occur in hadrons at high energies. These are expected to be reached in large accelerators such as LHC, HERA or RHIC. The solution to the BK equation including running coupling effects and a b-independent amplitude can predict correctly the values of structure functions of protons or DIS reduced cross section in four orders of Q^2. It is an integro-differential equation and it typically cannot be solved analytically.

The Balitsky-Kovchegov evolution equation was numerically solved using the Runge-Kutta method of fourth order, Simpson's rule and Lagrange interpolation. Various methods were tested and their initial parameters compared to obtain the best ratio of precision and computing speed since the program for solving the BK evolution equation is time demanding.

The optimal parameters to compute the BK equation for the case without impact parameter dependence prove to be the Runge-Kutta method of fourth order with a step of 0.01 in rapidity, Simpson's rule for the integration with step of 20 over the interval over θ_{rr_1} and 25 steps per order of magnitude of the dipole size r. A simple linear interpolation (in the log-scale) has been determined to give the best results since higher orders are not precise in certain regions and misshape the computed function. For the computation of the photon wave function, 10000 steps per the interval of $[0, 1]$ over the parameter z were chosen. This setup then enables us to compute the structure function up to the rapidity of $Y = 10$ in about 90 seconds on an average personal computer with a mean square error of $1.5\,\%$.

The shape of the photon wave functions was calculated and plotted with various factors that also take part in the final structure function computation. It was shown that the largest numerical contribution to the final value of the cross section and the structure function comes from the dipole size in interval $r \sim (0.1, 30)$ GeV^{-1} since the photon wave functions weighted by the solution of the BK evolution equation show negligible values outside this region and thus do not affect the final integral over r as much. The structure function F_2 and reduced cross section $\sigma_{T,L}$ were computed from the obtained solutions given by the rcBK equation for various values of Q^2 and compared to data measured at HERA.

The effect of geometric scaling, which is observed in solutions to the BK equation was also studied. Since the shape of the solutions changes only in the first few units of rapidity and then solely shifts towards lower values of r as the evolution propagated

towards higher values of Y, we were able to establish a new initial condition from the intrinsic properties of the BK equation itself. This geometrical scaled initial condition would then require less parameters that need to be fitted to data than the MV initial condition and could better reflect the physical nature of the system.

The geometrically scaled initial condition was obtained by running the computation up to the rapidity of $Y = 100$ and then re-scaling it back to the initial position. The functionality of this initial condition was then tested and the dependence of the results on the re-scaling parameter was studied. Its initial value was set as $Q_{s0}^2 = 0.07$ and the variation of this parameter later span from $Q_{s0}^2 = 0.03$ to $Q_{s0}^2 = 0.13$.

We searched to obtain a new value for the parameter σ_0 since in this approach, we are using a new initial condition and its value that was obtained in previous fits might not be accurate anymore. For this reason, values of F_2^{Data}/F_2^{Theory} were studied in order to obtain a correction factor for this constant. However the ratio of F_2^{Data}/F_2^{Theory} showed a logarithmically decreasing dependence on Q^2 for all choices of the re-scaling parameter. The slope of this decrease proved to be identical for all setups ($-0.07log(Q^2)$), just the added constant lowered as the saturation scale Q_{s0}^2 increased (from 0.7 to $0.45\,\mathrm{GeV}^2$). This effect has not yet been reported by other groups and its origin needs further explanation.

The quality of these fits was also tested by determining the value of χ^2. Its dependence on Q^2 was studied for various values the of re-scaling parameter. The lower values of Q_{s0}^2 exhibited worse χ^2 behavior in the regions with lower Q^2 than the fits obtained with higher Q_{s0}^2. Its values reached up to $\chi^2 = 3$ in the region $Q^2 \sim (1, 10)$ for $Q_{s0}^2 = 0.04\,\mathrm{GeV}^2$. The regions higher than $Q^2 = 30$ showed high values of χ^2 for all sets of re-scaling parameters, which might be caused by the fact that at these values of Q^2, the ratio F_2^{Data}/F_2^{Theory} has a non-trivial dependence on rapidity and that it cannot be fitted with a constant. This can mean that in this approach, there are still some softly contributing effects that have not yet been accounted for by the theory.

For $Q_{s0}^2 = 0.04\,\mathrm{GeV}^2$, the value of χ^2 reached the values of 7 at the highest at $Q^2 \sim 50\mathrm{GeV}^2$. As the re-scaling parameter increases, the value of χ^2 in this region further increases up to the maximal value of 14 when Q_{s0}^2 is set as $0.14\,\mathrm{GeV}^2$. The values of χ^2 reach high values towards higher Q^2, even though the growing trend of the ratio with respect to rapidity is slow, partly because the errorbars of the measured values decrease towards higher values of Q^2. In the intermediate values of Q^2, the values of χ^2 decrease with the increase of Q_{s0}^2 at first, but as we approach higher and higher values of Q_{s0}^2 its values are also distorted, so the optimal choice of the re-scaling parameter indeed proved to be $Q_{s0}^2 = 0.07\,\mathrm{GeV}^2$.

We used the obtained scaled initial condition to predict the values of the structure function $F_2(Q^2, Y)$ in regions that were not yet measured and where it differs from the solutions obtained with the MV initial condition. This prediction can then be used to determine the validity of this approach to the dipole model and rcBK equation in particular when new measurements (possibly at the LHC) are carried out.

Bibliography

[1] V. S. Fadin, E. A. Kuraev, and L. N. Lipatov, "On the Pomeranchuk Singularity in Asymptotically Free Theories," *Phys. Lett.*, vol. B60, pp. 50–52, 1975.

[2] L. N. Lipatov, "Reggeization of the Vector Meson and the Vacuum Singularity in Nonabelian Gauge Theories," *Sov. J. Nucl. Phys.*, vol. 23, pp. 338–345, 1976, [Yad. Fiz.23,642(1976)].

[3] E. A. Kuraev, L. N. Lipatov, and V. S. Fadin, "Multi - Reggeon Processes in the Yang-Mills Theory," *Sov. Phys. JETP*, vol. 44, pp. 443–450, 1976, [Zh. Eksp. Teor. Fiz.71,840(1976)].

[4] E. Kuraev, L. Lipatov, and V. S. Fadin, "The Pomeranchuk Singularity in Nonabelian Gauge Theories," *Sov.Phys.JETP*, vol. 45, pp. 199–204, 1977.

[5] I. Balitsky and L. Lipatov, "The Pomeranchuk Singularity in Quantum Chromodynamics," *Sov.J.Nucl.Phys.*, vol. 28, pp. 822–829, 1978.

[6] I. Balitsky, "Operator expansion for high-energy scattering," *Nucl. Phys.*, vol. B463, pp. 99–160, 1996.

[7] ——, "Factorization for high-energy scattering," *Phys. Rev. Lett.*, vol. 81, pp. 2024–2027, 1998.

[8] ——, "Factorization and high-energy effective action," *Phys. Rev.*, vol. D60, p. 014020, 1999.

[9] ——, "Effective field theory for the small x evolution," *Phys. Lett.*, vol. B518, pp. 235–242, 2001.

[10] Y. V. Kovchegov, "Small x F(2) structure function of a nucleus including multiple pomeron exchanges," *Phys. Rev.*, vol. D60, p. 034008, 1999.

[11] V. N. Gribov and L. N. Lipatov, "e+ e- pair annihilation and deep inelastic e p scattering in perturbation theory," *Sov. J. Nucl. Phys.*, vol. 15, pp. 675–684, 1972, [Yad. Fiz.15,1218(1972)].

[12] ——, "Deep inelastic e p scattering in perturbation theory," *Sov. J. Nucl. Phys.*, vol. 15, pp. 438–450, 1972, [Yad. Fiz.15,781(1972)].

[13] L. N. Lipatov, "The parton model and perturbation theory," *Sov. J. Nucl. Phys.*, vol. 20, pp. 94–102, 1975, [Yad. Fiz.20,181(1974)].

[14] Y. L. Dokshitzer, "Calculation of the Structure Functions for Deep Inelastic Scattering and e+ e- Annihilation by Perturbation Theory in Quantum Chromodynamics." *Sov. Phys. JETP*, vol. 46, pp. 641–653, 1977, [Zh. Eksp. Teor. Fiz.73,1216(1977)].

[15] G. Altarelli and G. Parisi, "Asymptotic Freedom in Parton Language," *Nucl. Phys.*, vol. B126, pp. 298–318, 1977.

[16] D. Strozik-Kotlorz, S. V. Mikhailov, and O. V. Teryaev, "Generalized DGLAP evolution," *J. Phys. Conf. Ser.*, vol. 678, no. 1, p. 012017, 2016.

[17] Z. Nagy and D. E. Soper, "Final state dipole showers and the DGLAP equation," *JHEP*, vol. 05, p. 088, 2009.

[18] D. Toton, "Gluon distributions from Oliveira-Martin-Ryskin combined BFKL+DGLAP evolution equations," *Phys. Rev.*, vol. D91, no. 5, p. 054003, 2015.

[19] J. L. Albacete and Y. V. Kovchegov, "Solving high energy evolution equation including running coupling corrections," *Phys. Rev.*, vol. D75, p. 125021, 2007.

[20] J. L. Albacete, N. Armesto, J. G. Milhano, and C. A. Salgado, "Non-linear QCD meets data: A Global analysis of lepton-proton scattering with running coupling BK evolution," *Phys. Rev.*, vol. D80, p. 034031, 2009.

[21] J. L. Albacete, N. Armesto, J. G. Milhano, P. Quiroga-Arias, and C. A. Salgado, "AAMQS: A non-linear QCD analysis of new HERA data at small-x including heavy quarks," *Eur. Phys. J.*, vol. C71, p. 1705, 2011.

[22] J. Cepila and J. G. Contreras, "Rapidity dependence of saturation in inclusive HERA data with the rcBK equation," 2015.

[23] M. Matas, J. Cepila, and J. G. Contreras, "Numerical precision of the solution to the running-coupling Balitsky-Kovchegov equation," *EPJ Web of Conferences*, vol. 112, p. 02008, 2016.

[24] A. M. Stasto, K. J. Golec-Biernat, and J. Kwiecinski, "Geometric scaling for the total gamma* p cross-section in the low x region," *Phys. Rev. Lett.*, vol. 86, pp. 596–599, 2001.

[25] M. Praszalowicz and T. Stebel, "Quantitative Study of Different Forms of Geometrical Scaling in Deep Inelastic Scattering at HERA," *JHEP*, vol. 04, p. 169, 2013.

[26] G. Soyez, C. Marquet, and R. B. Peschanski, "Geometric scaling in high-energy QCD at nonzero momentum transfer," in *Proceedings, 40th Rencontres de Moriond on QCD and High Energy Hadronic Interactions: La Thuile, Aosta Valley, Italy, March 12-19, 2005*, 2005, pp. 371–374. [Online]. Available: https://inspirehep.net/record/680565/files/arXiv:hep-ph_0504117.pdf

[27] A. Kormilitzin, E. Levin, and S. Tapia, "Geometric scaling behavior of the scattering amplitude for DIS with nuclei," *Nucl. Phys.*, vol. A872, pp. 245–264, 2011.

[28] K. J. Golec-Biernat and A. M. Stasto, "On solutions of the Balitsky-Kovchegov equation with impact parameter," *Nucl. Phys.*, vol. B668, pp. 345–363, 2003.

[29] J. Berger and A. M. Stasto, "Small x nonlinear evolution with impact parameter and the structure function data," *Phys. Rev.*, vol. D84, p. 094022, 2011.

[30] J. Berger and A. Stasto, "Numerical solution of the nonlinear evolution equation at small x with impact parameter and beyond the LL approximation," *Phys. Rev.*, vol. D83, p. 034015, 2011.

[31] M. H., "Balitsky-Kovchegov equation," *University of Jyvaskyla*, pp. 1–69, 2011.

[32] L. McLerran, "The CGC and the Glasma: Two Lectures at the Yukawa Insitute," *Prog. Theor. Phys. Suppl.*, vol. 187, pp. 17–30, 2011.

[33] M. Kuhlen, "QCD at HERA: The hadronic final state in deep inelastic scattering," *Springer Tracts Mod. Phys.*, vol. 150, pp. 1–172, 1999.

[34] V. Barone and E. Predazzi, *High-Energy Particle Diffraction*, ser. Texts and Monographs in Physics. Berlin Heidelberg: Springer-Verlag, 2002, vol. v.565. [Online]. Available: http://www-spires.fnal.gov/spires/find/books/www?cl=QC794.6.C6B37::2002

[35] N. N. Nikolaev and B. Zakharov, "Color transparency and scaling properties of nuclear shadowing in deep inelastic scattering," *Z. Phys.*, vol. C49, pp. 607–618, 1991.

[36] ——, "Pomeron structure function and diffraction dissociation of virtual photons in perturbative QCD," *Z. Phys.*, vol. C53, pp. 331–346, 1992.

[37] A. H. Mueller, "Small x Behavior and Parton Saturation: A QCD Model," *Nucl. Phys.*, vol. B335, p. 115, 1990.

[38] E. Iancu, K. Itakura, and S. Munier, "Saturation and BFKL dynamics in the HERA data at small x," *Phys. Lett.*, vol. B590, pp. 199–208, 2004.

[39] E. Gotsman, E. Levin, M. Lublinsky, and U. Maor, "Towards a new global QCD analysis: Low x DIS data from nonlinear evolution," *Eur. Phys. J.*, vol. C27, pp. 411–425, 2003.

[40] H. Kowalski and D. Teaney, "An Impact parameter dipole saturation model," *Phys. Rev.*, vol. D68, p. 114005, 2003.

[41] J. L. Albacete and C. Marquet, "Gluon saturation and initial conditions for relativistic heavy ion collisions," *Prog. Part. Nucl. Phys.*, vol. 76, pp. 1–42, 2014.

[42] K. J. Golec-Biernat and M. Wusthoff, "Saturation effects in deep inelastic scattering at low Q**2 and its implications on diffraction," *Phys. Rev.*, vol. D59, p. 014017, 1998.

[43] K. Nakamura *et al.*, "Review of particle physics," *J. Phys.*, vol. G37, p. 075021, 2010.

[44] P. Quiroga-Arias, J. L. Albacete, N. Armesto, J. G. Milhano, and C. A. Salgado, "AAMQS: a non-linear QCD description of new HERA data at small-x," *J. Phys.*, vol. G38, p. 124124, 2011.

[45] O. E.G., "Balitsky Kovchegov evolution equation," *Universidade Federal do Rio Grande do Sul.*, pp. 1–69,[online] http://www.if.ufrgs.br/gfpae/sem/2008/BK.pdf, 2009.

[46] J. Zhou, "The evolution of the small x gluon TMD," 2016.

[47] S. Fleming, "Glauber Gluons in SCET and the BFKL Equation," *PoS*, vol. QCDEV2015, p. 047, 2016.

[48] V. T. Kim, "Search for BFKL-evolution manifestations at high energies," *Int. J. Mod. Phys. Conf. Ser.*, vol. 39, p. 1560106, 2015.

[49] Y. V. Kovchegov, "Unitarization of the BFKL pomeron on a nucleus," *Phys. Rev.*, vol. D61, p. 074018, 2000.

[50] D. Boer, A. Utermann, and E. Wessels, "Compatibility of phenomenological dipole cross sections with the Balitsky-Kovchegov equation," *Phys. Rev.*, vol. D75, p. 094022, 2007.

[51] I. Balitsky, "Quark contribution to the small-x evolution of color dipole," *Phys. Rev.*, vol. D75, p. 014001, 2007.

[52] C. Marquet and G. Soyez, "The Balitsky-Kovchegov equation in full momentum space," *Nucl. Phys.*, vol. A760, pp. 208–222, 2005.

[53] Y. V. Kovchegov and H. Weigert, "Triumvirate of Running Couplings in Small-x Evolution," *Nucl. Phys.*, vol. A784, pp. 188–226, 2007.

[54] K. A. Olive *et al.*, "Review of Particle Physics," *Chin. Phys.*, vol. C38, p. 090001, 2014.

[55] L. D. McLerran and R. Venugopalan, "Boost covariant gluon distributions in large nuclei," *Phys. Lett.*, vol. B424, pp. 15–24, 1998.

[56] F. D. Aaron *et al.*, "Combined Measurement and QCD Analysis of the Inclusive e+- p Scattering Cross Sections at HERA," *JHEP*, vol. 01, p. 109, 2010.